Kinetic and Spectroscopic Evidence for Reaction Pathways and Intermediates for Olefin Epoxidation on Nb in *BEA

Supporting Information

Daniel T. Bregante[1], Pranjali Priyadarshini[1], and David W. Flaherty[1,*]

[1]Department of Chemical and Biomolecular Engineering
University of Illinois Urbana-Champaign, Urbana, IL 61801

*Corresponding Author

Phone: (217) 244-2816

Email: dwflhrty@illinois.edu

S1. Catalyst Characterization

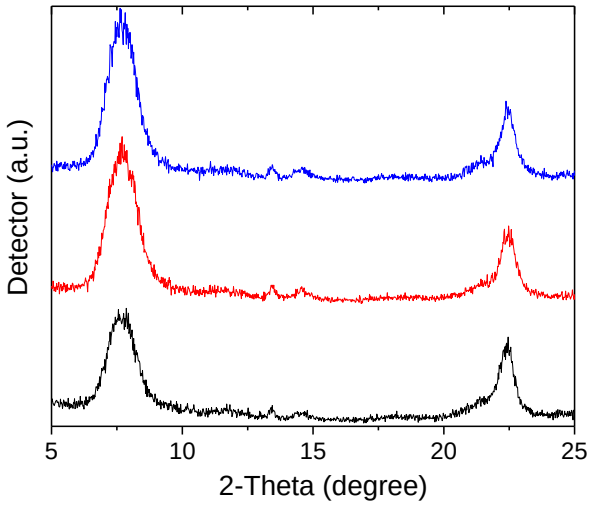

Figure S1. Powder X-ray diffractograms (p-XRD) for commercial Al-β (─, black), Si-β (─, red), and $Nb_{1.5}$-β (─, blue). P-XRD spectra were recorded under an ambient atmosphere using Cu K-α radiation (0.15418 nm) with a step size of 0.02° at 1° min^{-1}

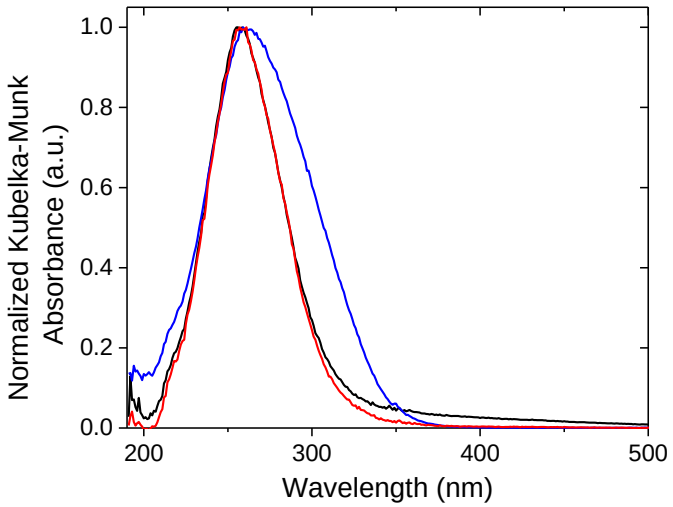

Figure S2. Diffuse reflectance UV-visible spectra for $Nb_{0.7}$-β (—), $Nb_{1.5}$-β (—), and 10 wt. % Nb-SiO_2 (—) normalized to the maximum feature. MgO was used as a reference to collect a total reflectance background spectrum. $Nb_{0.15}$-β was omitted and did not have a band edge calculated because its low absorbance yielded a noisy signal.

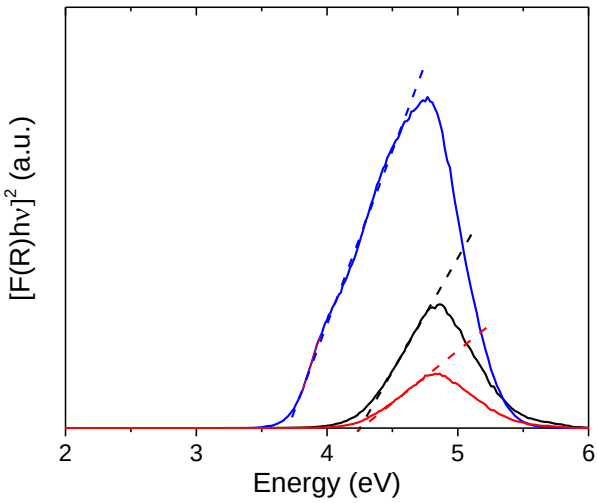

Figure S3. Tauc plots (where F(R) is the Kubelka-Munk absorbance function and hν is the energy of the photon) for $Nb_{0.7}$-β (—), $Nb_{1.5}$-β (—), and 10 wt % Nb-SiO_2 (—) using the DRUV-vis data from Figure S1.2. Dotted lines (with respective color) represents the fit to determine the band edge for each material.

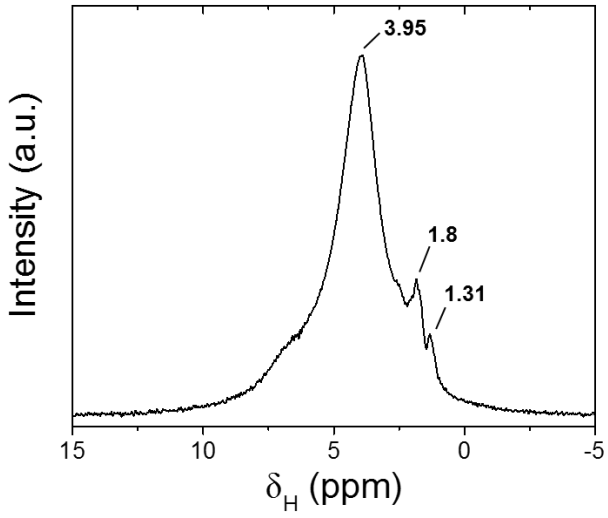

Figure S4. ^{1}H MAS NMR spectra obtained for $Nb_{1.5}$-β, recorded at ambient conditions in a 4 mm diameter zirconia rotor (10 kHz, 32 scans, 10 sec recycle delay).

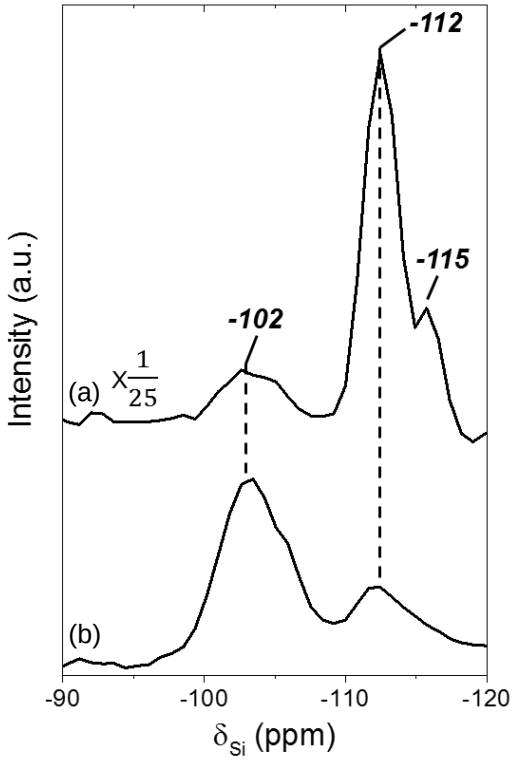

Figure S5. ^{29}Si MAS NMR spectra of $Nb_{1.5}$-β with (a) $^{1}H \rightarrow ^{29}Si$ cross or (b) ^{29}Si direct polarization recorded at ambient conditions in a 4 mm diameter zirconia rotor

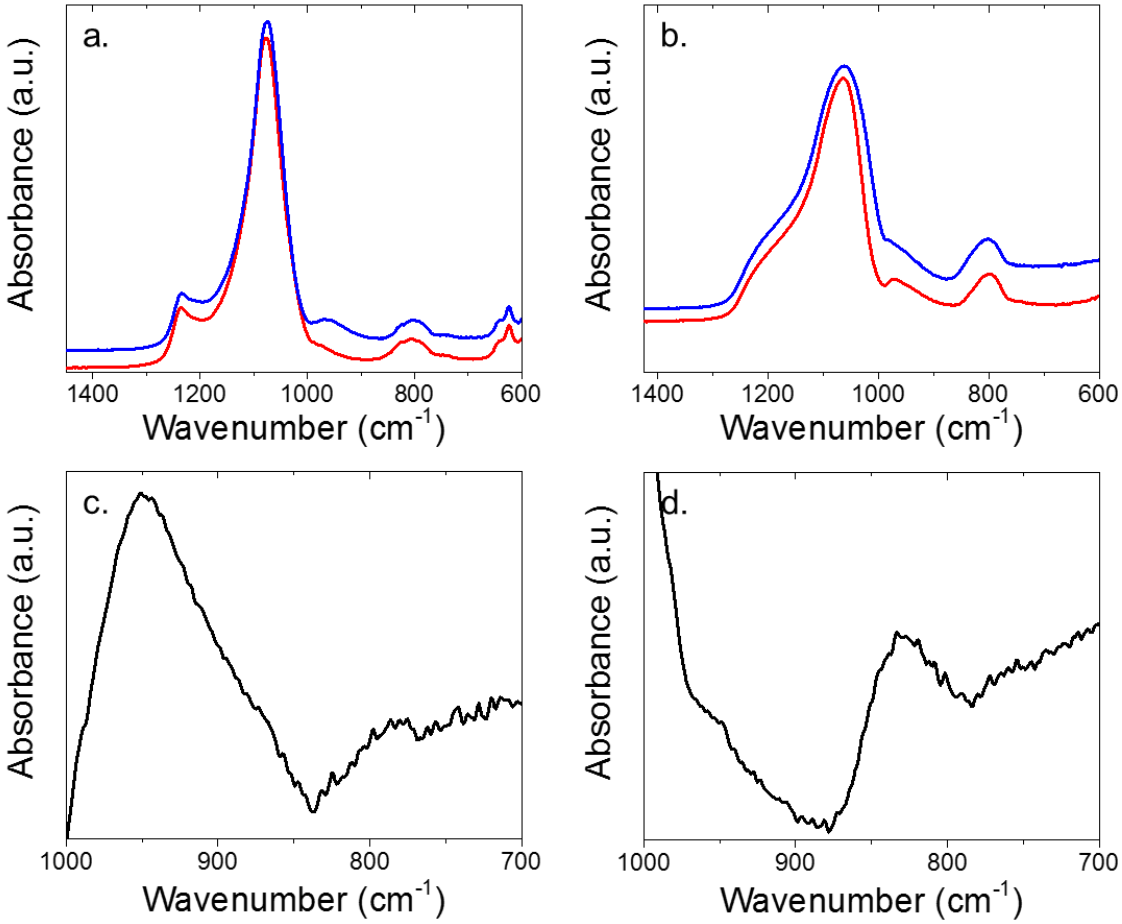

Figure S6. Normalized ATR-IR spectra of (a) Si-β (red, -) and $Nb_{1.5}$-β (blue, -), (b) SiO_2 (red, -) and $Nb_{10.0}$-SiO_2 (blue, -), (c) difference spectra of $Nb_{1.5}$-β with respect to Si-β, and (d) difference spectra of $Nb_{10.0}$-SiO_2 with respect to SiO_2. Spectra were acquired at ambient conditions with FTIR spectrometer (Bruker Alpha) equipped with a diamond ATR-IR accessory.

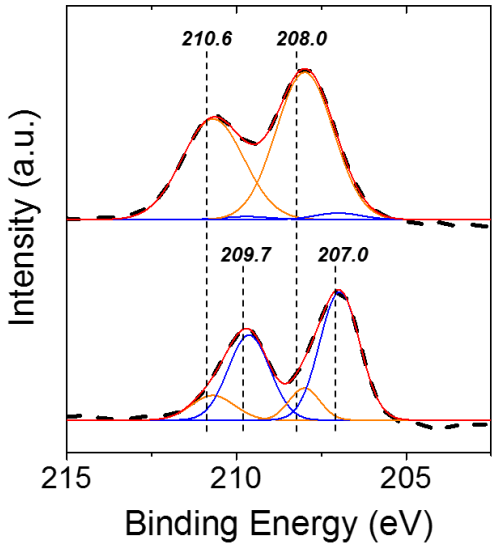

Figure S7. X-ray photoelectron spectra (black, dashed) of the Nb 3d region with peak fittings (colored, solid) for (a) untreated $Nb_{5.0}$-β and (b) H_2O_2-treated $Nb_{5.0}$-β. The peak fittings from the different oxidation states are color-coded for clarity: Nb^{IV} (blue, -), Nb^{V} (orange, -), and cumulative peak fit (red, -). Spectra are referenced to an aliphatic C 1s feature at 284.8 eV. The H_2O_2 treatment procedure is described in section 2.4.

Figure S7a (top curve) contains two large features (orange curves) at 210.6 and 208 eV, which are attributed to the Nb 3d 3/2 and 5/2 electrons for Nb^{V}, while the corresponding Nb^{IV} features (blue curves) are negligible in magnitude. While in contrast, Fig. S7b (bottom curve), contains two doublet features that correspond to both Nb^{V} and Nb^{IV} features, which would be expected for the Nb^{V}-OOH/Nb^{V}-$(O_2)^{2-}$ (i.e., hydroperoxide and peroxide) and Nb^{IV}-$(O_2)^{-}$ (i.e., superoxide) species, respectively.

S2. Control Experiments to Test Importance of Mass-Transfer Restrictions

Figure S2.1 Shows cyclohexene oxide formation measured as a function of cyclohexene concentration for multiple metal loads of Nb in Nb-β. The slope is independent of metal loading at all metal loadings tested (0.15, 0.7, 1.5 wt%), indicating that the Madon-Boudart criterion [1] is satisfied for Nb-β catalysts used to determine the kinetics of the reaction. Within Figure S7, the maximum difference in turnover rate values ($7.5 \cdot 10^{-5}$ (mol $C_6H_{10}O$)(mol Nb·s)$^{-1}$) is within the maximum observed error for these reactions (< 7% error). Moreover, the differences between the turnover rates on these catalysts are not systematic across the range of cyclohexene concentrations, which indicates that these differences result from random error. Thus, we do not interpret any minute changes in turnover rates as an indicator about a change in the catalyst structure.

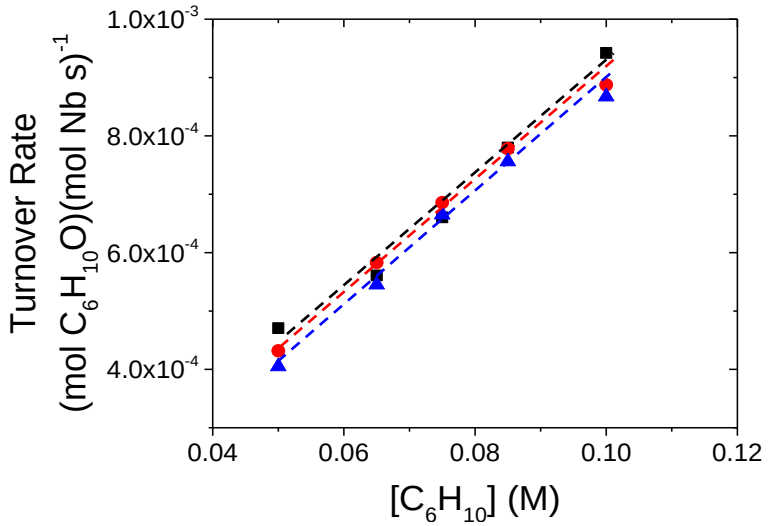

Figure S8. $C_6H_{10}O$ turnover rates as a function of $[C_6H_{10}]$ in 1mM H_2O_2 with $Nb_{1.5}$-β (■), $Nb_{0.7}$-β (●) and $Nb_{0.15}$-β (▲) (30 mg catalyst, 30 cm^3 CH_3CN, 313 K). Lines are intended to guide the eye.

S3. In Situ UV-vis Spectroscopy

S3.1 Data Acquisition and Processing

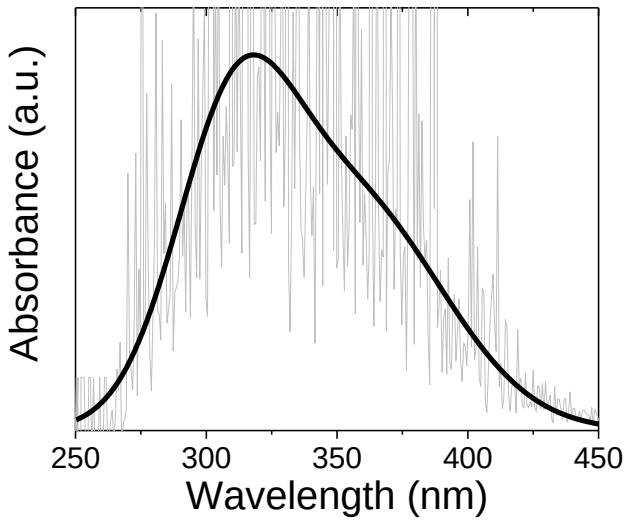

Figure S9. UV-vis absorbance spectrum (raw data, –) of H_2O_2-treated $Nb_{0.3}$-β at 313 K in flowing CH_3CN (0.4 M H_2O) and smoothed data (–) using a finite fourier transform with 40 points of smoothing between 250 and 500 nm. Data smoothing performed in OriginPro®.

S3.2 Kinetic Parameter Optimization

Scheme 1. Proposed mechanism for the formation of Nb-OOH and Nb-$(O_2)^-$ with interconversion between the two proposed intermediates followed by epoxidation of C_2H_4.

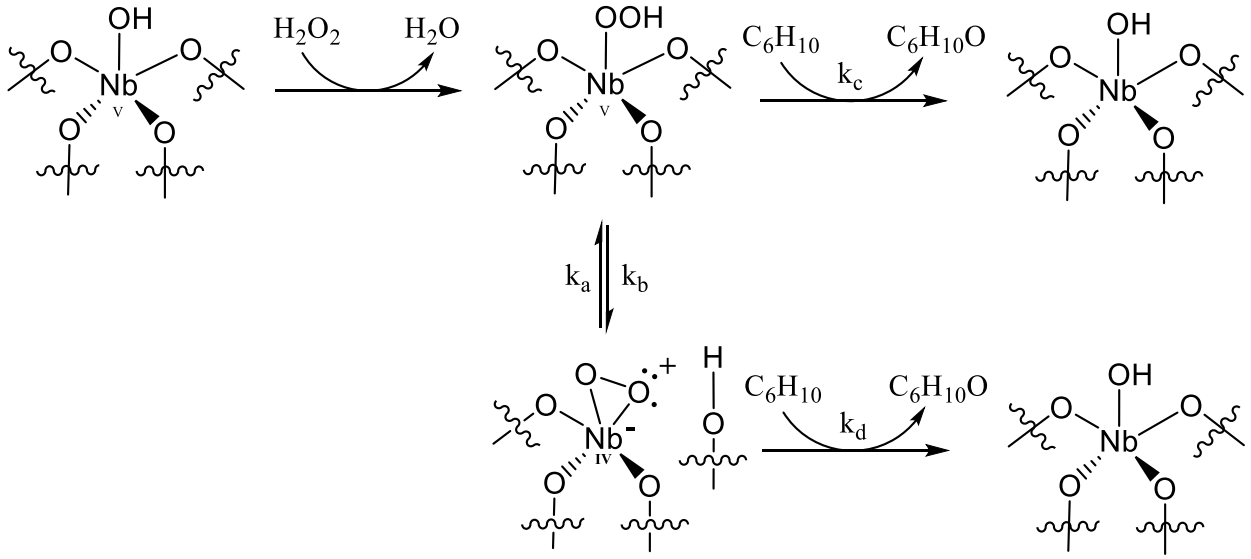

[a]Formation of Nb-OOH and Nb-$(O_2)^-$ occurs during the activation of H_2O_2 over $Nb_{1.5}$-β with subsequent drying steps to remove formed and adsorbed H_2O (Section 2.4).

The ODE45 function in MATLAB™ was used to simultaneously solve equations 2 and 3 (from the main text) with an initial guess for the kinetic parameters (i.e., k_a, k_b, k_c, and k_d, Scheme S1). The sum of the square of the differences between the solution of the two coupled differential equation and the experimental data was used to calculate a residual value. The "fmincon" function was used with a lower bound of 0 for all parameters to optimize the k_a, k_b, k_c, and k_d values to minimize the residual between the simulated differential equations and our experimental data. The initial guess used was 0.01, 0.01, 0.001, and 0.001 for k_a, k_b, k_c, and k_d, respectively. Changes of each of the values by an order of magnitude (increasing and decreasing) led to the same optimized results, which suggests that the fit values for rate constants are not in a local minimum in solution space. As such, the unconstrained solution is presumed to be correct (Table 3), as there is no evidence for Nb-OOH being inactive for consumption by reaction with C_6H_{10}; while the high ratio of k_d to k_c (i.e., ~ $2 \cdot 10^4$) strongly suggests that Nb-$(O_2)^-$ is the active intermediate for olefin epoxidation.

S4. In Situ FTIR Spectroscopy

S4.1. MES-PSD Data Analysis

The raw time-resolved FTIR spectra is collected and processed through various mathematical steps before analysis. The time-domain raw spectra is first averaged onto a single period using:

$$A_{average}(t) = \frac{T}{T_{total}} \sum_{i=0}^{\frac{T_{total}}{T}} A(t + iT) \quad (S4.1)$$

where $A(t + iT)$ is the absorbance at each time point, $A_{average}(t)$ is the absorbance after averaging into a single period, T is the time period of stimulation, and T_{total} is the total time for which the experiment was run. Hence, $\frac{T_{total}}{T}$ represents the total number of periods of stimulations for which an experiment was run. The averaged spectra is then subjected to demodulation by phase sensitive detection (PSD) using:

$$A_k(\varphi_k^{PSD}) = \frac{2}{T} \int_0^T A_{average}(\vartheta, t) \sin(k\omega t + \varphi_k^{PSD}) dt, \quad (S4.2)$$

Equation S4.2 is transformed into a Fourier series by Fourier's theorem for a periodic function:

$$A(\vartheta, t) = \sum_{i=1}^{N} A_{i,0}(\vartheta) + \sum_{i=1}^{N} \sum_{k=1}^{\infty} \left(A_{i,k}^{0^\circ}(\vartheta) \cos k\omega t + A_{i,k}^{90^\circ}(\vartheta) \sin k\omega t \right) \quad (S4.3)$$

where $A_{i,0}$ is the dc component, and $A_{i,k}^{0^\circ}$ and $A_{i,k}^{90^\circ}$ are the orthogonal components of the vector.

Each of the above terms in the integral is converted into a single equation using Simpson's Rule:

$$\int_0^T y(t) dt = \frac{\Delta t}{3} (y_0 + 4y_1 + 2y_2 + 4y_3 + \cdots + 2y_{n-2} + 4y_{n-1} + y_n) = \frac{\Delta t}{3} \sum_{i=0}^{n} s_i y_i \quad (S4.4)$$

where s_i, is Simpson's coefficient (where n must be an even number). A detailed mathematical derivation and implications were discussed in details by Baurecht et. al. [2]. A self-developed code in MATLAB™ was used to resample the acquired spectra and perform the phase sensitive detection analysis using equations S4.1-S4.4.

S4.2. Verification of Sinusoidal Reactant Modulation

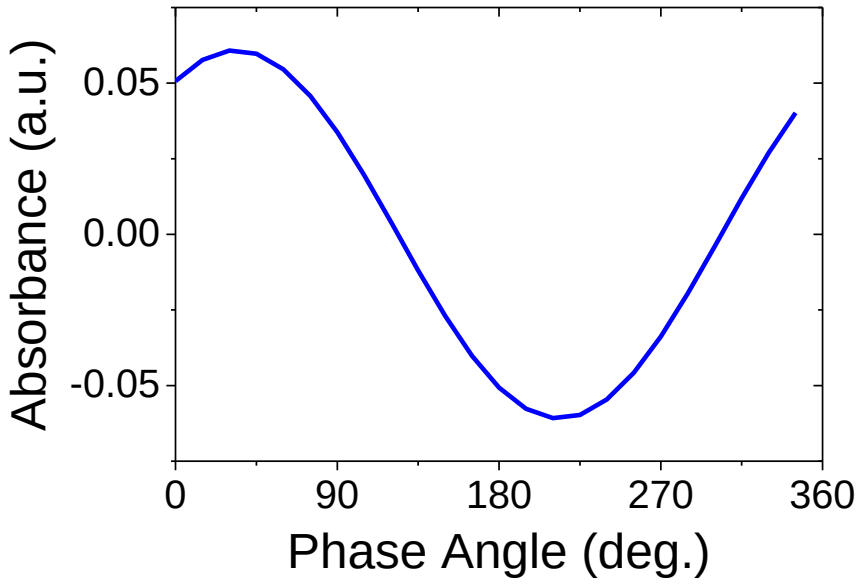

Figure S10. Infrared absorbance value at 1630 cm^{-1} (bending mode of liquid H_2O) as a function of phase angle obtained while sinusoidally modulating the flowrates of C_6H_{10} (0.1 M C_6H_{10} in CH_3CN) and H_2O_2 (0.065 M H_2O_2 in CH_3CN, i.e., H_2O-free liquid stream) solutions (0.5 cm^3 total volumetric flowrate, 333 K, Section 2.5)

S.4.3. Steady-State FTIR Spectra Showing Stability of Nb-(O_2)* Species

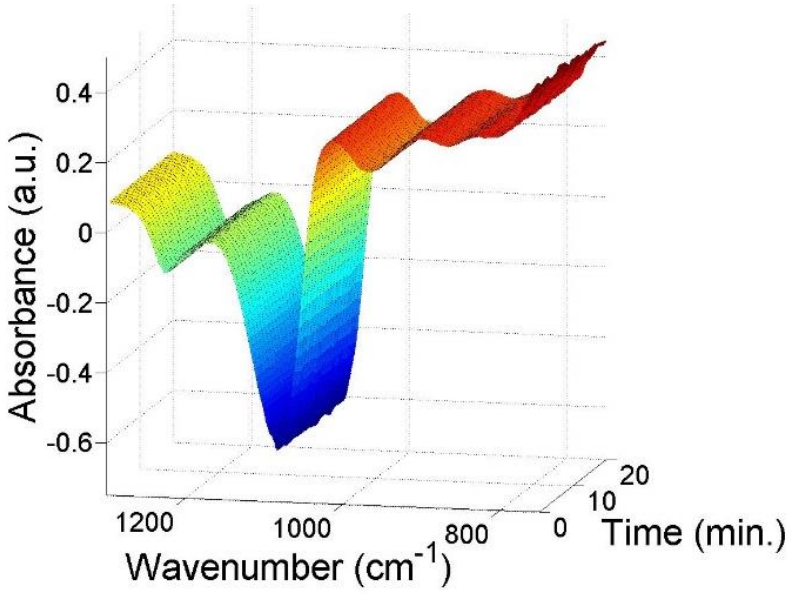

Figure S11. Time-resolved in situ IR spectra showing stability of Nb-$(O_2)^-$ and Nb-OOH after contact with flowing H_2O_2 (Fig. 3a), while DI H_2O flow (0.5 cm^3 min^{-1}) was initiated at 333 K.

S.4.3. Proposed Mechanism for Olefin Epoxidation with Nb-$(O_2)^-$

Scheme S2. Proposed bi-radical pathway for the epoxidation of cyclohexene by Nb-$(O_2)^-$, similar to those proposed for epoxidation with homogeneous vanadium complexes [3, 4].

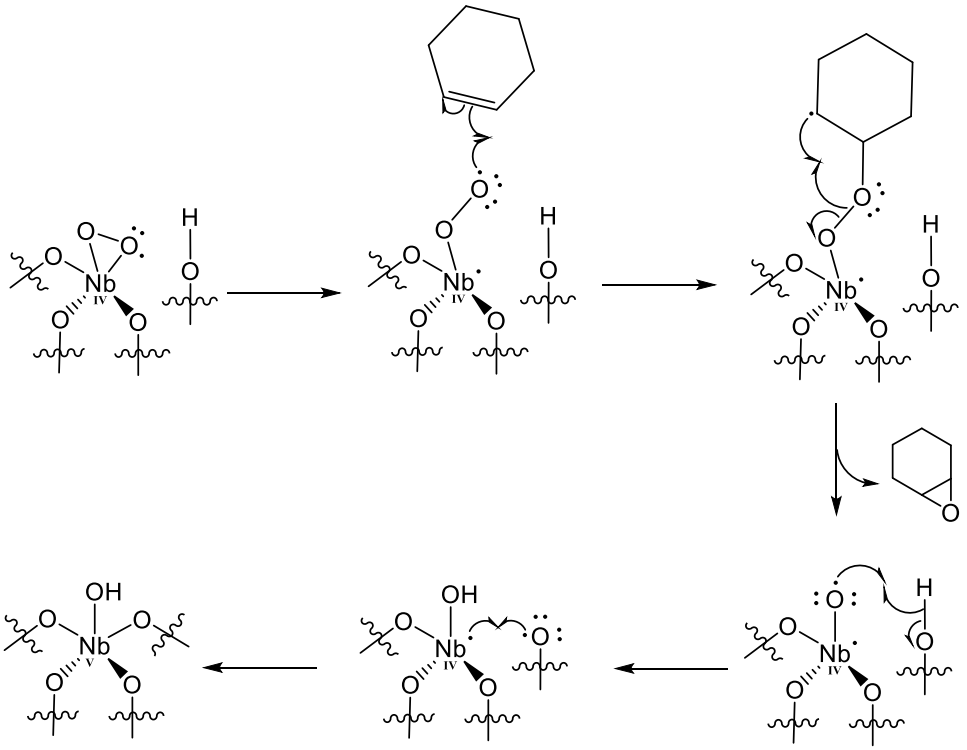

S5. Previously Proposed Mechanisms for Olefin Epoxidation [5-7]

Previous models for olefin epoxidation on metal-oxide catalysts (i.e., TS-1 [7] and Ta [5, 6] grafted onto silica) are inconsistent with the experimental data obtained for C_6H_{10} epoxidation over Nb-β, specifically, these previous models assume quasi-equilibrated (QE) formation of a reactive intermediate (i.e., Ti- or Ta-(O_2)*) which does not encompass the observed dependence on epoxide concentration, likely because these studies did not test for oxygenate (e.g., epoxide) dependencies.

A reactive intermediate (Nb-$(O_2)^-$) reacts with C_6H_{10} in solution (Scheme 1, step 4) to yield the following rate expression:

$$r_E = k_4[C_6H_{10}][Nb-(O_2)^-] \tag{S5.1}$$

where r_E is the turnover rate of $C_6H_{10}O$ formation, $[Nb-(O_2)^-]$ is the number of Nb-$(O_2)^-$, and k_4 is the rate constant for the epoxidation of C_6H_{10} with Nb-(O_2)*. When adsorption of the olefin, H_2O_2, epoxide, and the formation of a reactive intermediate are all assumed to be QE with olefin epoxidation being kinetically relevant (KR), the following rate equation emerges:

$$r_E = \frac{(k_4K_2K_3K_5[C_6H_{10}][H_2O_2])}{[H_2O]}\ [*] \tag{S5.2}$$

where k_x and K_x are the rate and equilibrium constants, respectively, for each step x and [*] is the number of available Nb-OH moieties (i.e. active sites) that bind and react with species in solution. An expression for [*] is given from summing the number of likely surface intermediates:

$$[L] = [*] + [C_6H_{10}*] + [H_2O_2*] + [Nb-(O_2)^-] + [C_6H_{10}O*] \tag{S5.3}$$

where $[L]$ is the total number of active sites and $[C_6H_{10}*]$, $[H_2O_2*]$, and $[C_6H_{10}O*]$ are adsorbed C_6H_{10}, H_2O_2, and $C_6H_{10}O$ species, respectively, and $[Nb-(O_2)^-]$ is the reactive intermediate. Equation S5.3 can then be re-expressed in terms of the rate and equilibrium constants as well as the reactant concentrations:

$$[L] = ([*] + K_1[C_6H_{10}][*] + K_2K_3[H_2O_2][*] + K_5[C_6H_{10}O][*]) \tag{S5.4}$$

The combination of equations S5.2 and S5.4 yield the complete rate expression for $C_6H_{10}O$ formation:

$$\frac{r_E}{[L]} = \frac{k_4K_2K_3K_5[C_6H_{10}][H_2O_2]}{[H_2O](1+K_1[C_6H_{10}]+K_2K_3[H_2O_2]+K_5[C_6H_{10}O])} \tag{S5.5}$$

Active sites become saturated with H_2O_2-derived intermediates (i.e. H_2O_2 or Nb-$(O_2)^-$ is the MASI) in the limit of low $[C_6H_{10}]$:$[H_2O_2]$, reducing the rate expression to

$$\frac{r_E}{[L]} = \frac{k_4K_5[C_6H_{10}]}{[H_2O]} \tag{S5.6}$$

Equation 6 is consistent with the $C_6H_{10}O$ formation rates that increase in proportion to $[C_6H_{10}]$ at low $[C_6H_{10}]$:$[H_2O_2]$ (Figure 3a, 0.01 – 0.1 M C_6H_{10}), and which do not depend on $[H_2O_2]$ (Figure 3b, 0.5 – 5 mM H_2O_2, 5 mM C_6H_{10}). The coverage of C_6H_{10} increases with $[C_6H_{10}]$ such that C_6H_{10}* becomes the MASI when $[C_6H_{10}]$ is greater than 0.5 M (when $[H_2O_2]$ is 1 mM), which causes equation S5.6 to take the form:

$$\frac{r_E}{[L]} = \frac{k_4 K_2 K_3 K_5 [H_2O_2]}{K_1 [H_2O]} \tag{S5.7}$$

This expression agrees with the $C_6H_{10}O$ formation rates seen in Fig. 5a, in that the rate of reaction is independent of $[C_6H_{10}]$. Additionally, equation S5.7 is in agreement with the results shown in Fig. 5b, where the turnover rate for epoxidation is proportional to $[H_2O_2]$ at high $[C_6H_{10}]$. Moreover, equations S5.5, S5.6, and S5.7 are identical to rate expressions derived previously for olefin epoxidations on similar metal-oxide catalysts.[5-7] However, the rate expressions obtained do not account for turnover rates for $C_6H_{10}O$ formation being inversely proportional to $C_6H_{10}O$ concentration. If $C_6H_{10}O$ is assumed to become the MASI at high $[C_6H_{10}]$, then equation S5.5 reduces to:

$$\frac{r_E}{[L]} = \frac{k_4 K_2 K_3 [C_6H_{10}][H_2O_2]}{K_5 [H_2O][C_6H_{10}O]} \tag{S5.8}$$

which possesses first-order dependence on $[C_6H_{10}]$.

S6. Rate Expression for H_2O_2 Decomposition by Nb-β

When Nb-$(O_2)^-$ undergoes a biomolecular reaction with H_2O_2 (Scheme 1, Step 6) the following rate expression is given as:

$$r_D = k_4[H_2O_2][Nb-(O_2)^-] \tag{S6.1}$$

where r_D is the rate of H_2O_2 decomposition, $[Nb-(O_2)^-]$ is the concentration of Nb-$(O_2)^-$, and k_6 is the rate constant for the decomposition of H_2O_2 with Nb-$(O_2)^-$. When we apply the observation (Section 3.3) that Nb-$(O_2)^-$ formation is irreversible, and all adsorption/desorption steps are QE we equation S6.1 becomes:

$$r_D = \frac{\left(k_6K_2K_3K_5[H_2O_2]^2\right)[*]}{\left(k_4K_5[C_6H_{10}]+k_6[H_2O_2]\right)} \tag{S6.2}$$

where k_x and K_x are the rate and equilibrium constants, respectively, for each step x and [*] is the number of available Nb-OH moieties (i.e. active sites) that bind and react with species in solution. An expression for [*] is given from summing the number of likely surface intermediates:

$$[L] = ([*]+[C_6H_{10}*]+[H_2O_2*]+[Nb-(O_2)*]+[C_6H_{10}O*]) \tag{S6.3}$$

where $[L]$ is the total number of active sites and $[C_6H_{10}*]$, $[H_2O_2*]$, and $[C_6H_{10}O*]$ are adsorbed C_6H_{10}, H_2O_2, and $C_6H_{10}O$ species, respectively, and Nb-$(O_2)^-$ is the reactive intermediate. Equation S6.3 can then be re-expressed in terms of the rate and equilibrium constants as well as the reactant concentrations:

$$[L] = \left([*]+K_1[C_6H_{10}][*]+K_2[H_2O_2][*]+\frac{k_3K_2[H_2O_2][*]}{\left(k_4K_5[C_6H_{10}]+k_6[H_2O_2]\right)}+K_5[C_6H_{10}O][*]\right) \tag{S6.4}$$

The combination of equations S6.2 and S6.4 yield the complete rate expression for H_2O_2 decomposition:

$$\frac{r_D}{[L]} = \frac{k_3k_6K_2[H_2O_2]^2}{\left(k_4K_5[C_6H_{10}]+k_6[H_2O_2]\right)\left(1+K_1[C_6H_{10}]+K_2[H_2O_2]+\frac{k_3K_2[H_2O_2]}{\left(k_4K_5[C_6H_{10}]+k_6[H_2O_2]\right)}+K_5[C_6H_{10}O]\right)} \tag{S6.5}$$

The form of this full rate equation simplifies in the limit when active sites become saturated with H_2O_2-derived intermediates (i.e. Nb-$(O_2)^-$ is the MASI) as is expected in the limit of low $[C_6H_{10}]$:$[H_2O_2]$:

$$\frac{r_D}{[L]} = k_6[H_2O_2] \tag{S6.6}$$

which shows that the apparent dependence on $[H_2O_2]$ for H_2O_2 decomposition is first order.

S7. H_2O_2 Selectivity as a Function of C_6H_{10} Concentration

H_2O_2 selectivities expressed as α values (the ratio of the turnover numbers for $C_6H_{10}O$ formation to that of H_2O_2 consumption) were calculated across the range of cyclohexene concentrations used in study. In general, H_2O_2 is used more selectively to form $C_6H_{10}O$ at the greatest C_6H_{10} to H_2O_2 ratios.

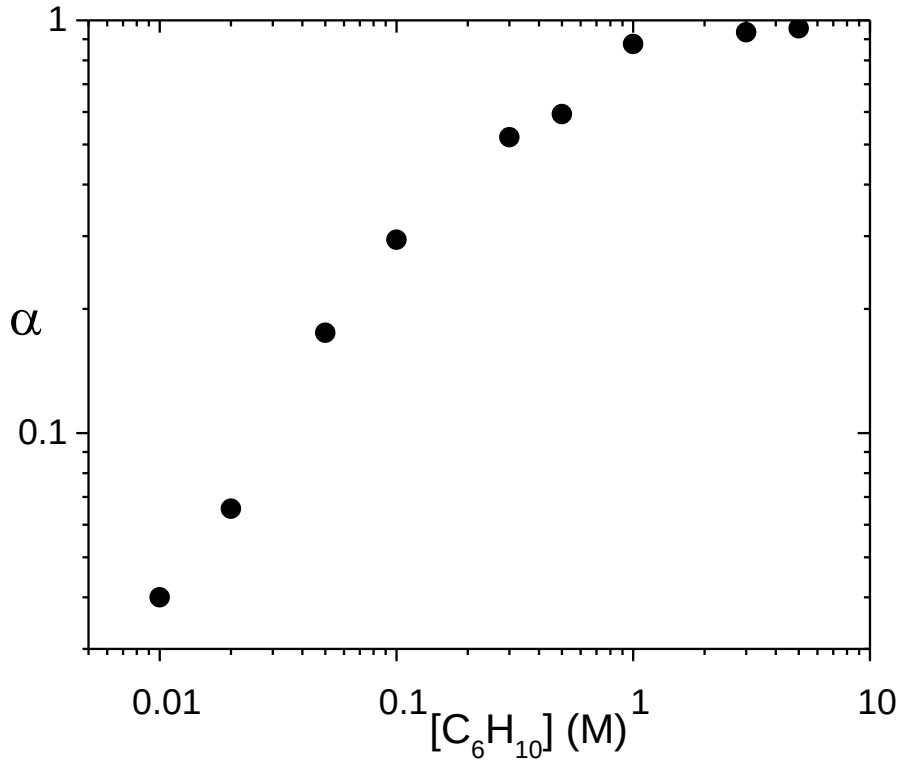

Figure S12. H_2O_2 selectivity (α, Section 3.4) for epoxidation as a function of $[C_6H_{10}]$ over $Nb_{1.5}$-β (1 mM H_2O_2, ~30 cm^3 CH_3CN, 313 K)

S8. Temperature Dependence of $C_6H_{10}O$ Formation and H_2O_2 Decomposition

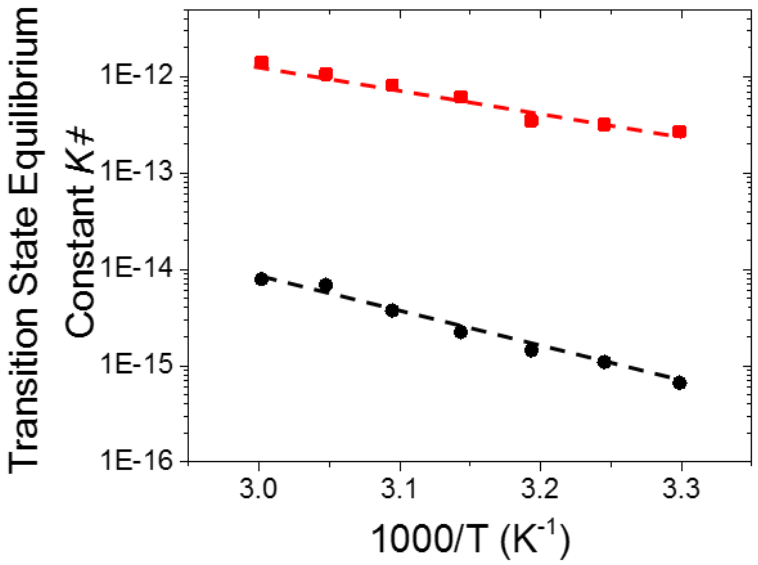

Figure S13. Transition state equilibrium constants, ($K^{\ddagger}$), for C_6H_{10} epoxidation (●) and H_2O_2 decomposition (■) as functions of inverse temperature on $Nb_{1.5}$-β (0.05 M C_6H_{10}, 1 mM H_2O_2) with a Nb-$(O_2)^-$ MASI. Error bars were omitted for clarity. In all reported rate data, error was < 10%. Lines represent fits to the Eyring equation (equation 23).

References:

[1] R.J. Madon, M. Boudart, Experimental Criterion for the Absence of Artifacts in the Measurement of Rates of Heterogeneous Catalytic Reactions, Ind. Eng. Chem. Fundam., 21 (1982) 438-447.

[2] D. Baurecht, U.P. Fringeli, Quantitative modulated excitation Fourier transform infrared pectroscopy, Rev. Sci. Instrum., 72 (2001) 3782.

[3] N.K.K. Raj, A.V. Ramaswamy, P. Manikandan, Oxidation of norbornene over vanadium-substituted hosphomolybdic acid catalysts and spectroscopic investigations, J. Mol. Catal. A: Chem., 227 (2005) 37-45.

[4] C.K. Sams, K.A. Jorgensen, Mechanistic Aspects of Vanadium-Catalysed Oxygen Transfer Reactions, Acta Chem. Scand., 49 (1995) 839-847.

[5] N. Morlanes, J.M. Notestein, Kinetic study of cyclooctene epoxidation with aqueous hydrogen peroxide over silica-supported calixarene–Ta(V), Applied Catalysis A: General, 387 (2010) 45-54.

[6] D.A. Ruddy, T.D. Tilley, Kinetics and Mechanism of Olefin Epoxidation with Aqueous H2O2 and a Highly Selective Surface-Modified TaSBA15 Heterogeneous Catalyst, Journal of the American Chemical Society, 130 (2008) 11088-11096.

[7] H. Gao, G. Lu, J. Suo, S. Li, Epoxidation of allyl chloride with hydrogen peroxide catalyzed by titanium silicalite 1, Appl. Catal., A, 138 (1996) 27-38.